

Isospin properties of quark matter from a 3-flavor NJL model

He Liu,^{1,2} Jun Xu*,¹ Lie-Wen Chen,^{3,4} and Kai-Jia Sun³

¹*Shanghai Institute of Applied Physics, Chinese Academy of Sciences, Shanghai 201800, China*

²*University of Chinese Academy of Sciences, Beijing 100049, China*

³*Department of Physics and Astronomy and Shanghai Key Laboratory for Particle Physics and Cosmology, Shanghai Jiao Tong University, Shanghai 200240, China*

⁴*Center of Theoretical Nuclear Physics, National Laboratory of Heavy Ion Accelerator, Lanzhou 730000, China*

(Dated: June 7, 2021)

We have studied the properties of hot and dense quark matter based on the 3-flavor Nambu-Jona-Lasinio (NJL) model as well as its Polyakov-loop extension (pNJL) with scalar-isovector and vector-isovector couplings. Provided a considerable large isospin asymmetry or isospin chemical potential, isospin splittings of constituent mass, chiral phase transition boundary, and critical point for u and d quarks can be observed for positive isovector coupling constants but are suppressed for negative ones. The quark matter symmetry energy decreases with the increasing isovector coupling constant, and is mostly enhanced in the pNJL model than in the NJL model. A positive scalar-isovector coupling constant is more likely to lead to an unstable isospin asymmetric quark matter. The isovector coupling has been further found to affect particle fractions as well as the equation of state in hybrid stars. Possible effects on the isospin properties of quark matter have also been discussed if the strangeness sector is further broken among the flavor symmetry.

PACS numbers: 21.65.Qr, 25.75.Nq, 21.65.Ef, 26.60.Kp

I. INTRODUCTION

The phase structure of quantum chromodynamics (QCD) matter in three dimensions, i.e., the temperature, the baryon chemical potential, and the isospin, is the holy grail of nuclear physics. So far great efforts have been made in understanding the QCD phase diagram at nearly zero isospin. For instance, the transition from the produced quark-gluon plasma (QGP) to hadronic matter at the top energy of the Relativistic Heavy Ion Collider (RHIC) or at the Large Hadron Collider (LHC) is a smooth crossover at nearly zero baryon and isospin chemical potential based on Lattice QCD (LQCD) studies [1–3]. Although LQCD suffers from the fermion sign problem [4–6] at finite baryon chemical potential, the hadron-quark phase transition can be a first-order one at large baryon chemical potentials based on studies from phenomenological theoretical models, e.g., the Nambu-Jona-Lasinio (NJL) model and its extensions [7–10]. To further explore the QCD phase structure and search for the signal of the critical point between the crossover and the first-order transition, experimental programs such as the Beam-Energy Scan (BES) at RHIC and the Compressed Baryonic Matter (CBM) at Facilities for Antiproton and Ion Research (FAIR) were proposed. However, using neutron-rich heavy-ion beams, the isospin degree of freedom is expected to be increasingly important at lower collision energies with larger net baryon densities. The different interactions for u quark and d quark in baryon-rich isospin asymmetric quark matter consisting of different net numbers of u and d quarks can lead to

isospin-dependent dynamics in the QGP. In addition, the phase boundary as well as the critical point extracted from these experiments are actually those at finite isospin in the 3-dimensional QCD phase diagram, since the whole system is a globally neutron-rich or d -quark-rich one.

The isospin physics has been in fact a hot topic in low-energy nuclear physics as well as nuclear astrophysics in the past 15 years, and the nuclear symmetry energy, the energy excess for neutron-rich system comparing with isospin symmetric one, is important in understanding various phenomena in finite nuclei, nuclear reactions, and compact stars [11–17]. Generally, a larger symmetry energy leads to a repulsive (attractive) potential for particles with negative (positive) isospin, and a stiffer equation of state (EOS) for isospin asymmetric matter. Besides the interesting isospin dynamics at RHIC-BES and FAIR-CBM and isospin dependent QCD phase diagram mentioned above, the quark matter symmetry energy, the EOS of the isospin asymmetric quark matter, and their temperature dependence are also interesting topics. The EOS of hot quark matter is the main ingredient for hydrodynamic calculation of the QGP evolution, while that of cold quark matter is important in understanding the properties of quark stars or hybrid stars, which is probably related to the recently observed massive compact stars, e.g., PSR J1614-2230 with $M = (1.97 \pm 0.04)M_{\odot}$ [18] and PSR J0348+0432 with $M = (2.01 \pm 0.04)M_{\odot}$ [19]. With the increasing temperature or density in heavy-ion systems or compact stars, strangeness can also be abundantly produced, and the isospin dependence of the system is often coupled with the strangeness sector.

In the present study, we explore the properties of isospin asymmetric quark matter based on a 3-flavor NJL model, which can successfully interpret the dynamics of

*corresponding author: xujun@sinap.ac.cn

spontaneous breaking of chiral symmetry in vacuum and its restoration at high temperatures and baryon chemical potentials, together with its Polyakov-loop extension (pNJL) which can describe the deconfinement phase transition. In order to study the isospin physics of quark matter, we break the SU(3) symmetry of the 3-flavor NJL Lagrangian by introducing the scalar-isovector and vector-isovector couplings [20], corresponding to different extent of isospin symmetry breaking in the scalar and vector channels. We will see that the isospin vector couplings may have dramatic effects on the isospin dependence of the QCD phase diagram at large isospin chemical potential as well as the quark matter symmetry energy. We have also explored the possible effects on the isospin dependence of the results if the strangeness sector is further broken among the flavor symmetry.

This paper is organized as follows. In Sec. II, we briefly review the formalism of the 3-flavor NJL model and pNJL model with isovector couplings. The effects of the isovector couplings on the phase diagram of isospin asymmetric quark matter and the quark matter symmetry energy are discussed in Secs. III and IV, and the properties of hybrid stars are discussed in Sec. V. The possible effects from further breaking of the strangeness sector on the obtained results are discussed in Sec. VI. A summary is given in Sec. VII.

II. THEORETICAL MODEL

By introducing the scalar-isovector coupling and the vector-isovector coupling, the Lagrangian of the 3-flavor NJL model can be written as

$$\begin{aligned}
\mathcal{L}_{\text{NJL}} = & \bar{q}(i\partial - \hat{m})q + \frac{G_S}{2} \sum_{a=0}^8 [(\bar{q}\lambda_a q)^2 + (\bar{q}i\gamma_5\lambda_a q)^2] \\
& + \frac{G_V}{2} \sum_{a=0}^8 [(\bar{q}\gamma_\mu\lambda_a q)^2 + (\bar{q}\gamma_5\gamma_\mu\lambda_a q)^2] \\
& - K \{ \det[\bar{q}(1 + \gamma_5)q] + \det[\bar{q}(1 - \gamma_5)q] \} \\
& + G_{IS} \sum_{a=1}^3 [(\bar{q}\lambda_a q)^2 + (\bar{q}i\gamma_5\lambda_a q)^2] \\
& + G_{IV} \sum_{a=1}^3 [(\bar{q}\gamma_\mu\lambda_a q)^2 + (\bar{q}\gamma_5\gamma_\mu\lambda_a q)^2], \quad (1)
\end{aligned}$$

where q denotes the quark fields with three flavors, i.e., u , d , and s , and three colors; $\hat{m} = \text{diag}(m_u, m_d, m_s)$ is the current quark mass matrix in flavor space; λ_a are the flavor SU(3) Gell-Mann matrices with $\lambda_0 = \sqrt{2/3}I$; G_S and G_V are the strength of the scalar and vector coupling, respectively; and the K term represents the six-point Kobayashi-Maskawa-t'Hooft (KMT) interaction that breaks the axial $U(1)_A$ symmetry. Since the Gell-Mann matrices with $a = 1 \sim 3$ are identical to the Pauli matrices in u and d space, the last two terms represent the scalar-isovector and vector-isovector coupling

breaking the SU(3) asymmetry while keeping the isospin symmetry, with G_{IS} and G_{IV} the corresponding coupling strength. In the present study, we employ the parameters $m_u = m_d = 3.6$ MeV, $m_s = 87$ MeV, $G_S\Lambda^2 = 3.6$, $K\Lambda^5 = 8.9$, and the cutoff value in the momentum integral $\Lambda = 750$ MeV given in Refs. [10, 21, 22]. G_V is set to 0 in the present study.

In the mean-field approximation, quarks can be taken as quasiparticles with constituent mass M_i given by the gap equation as

$$M_i = m_i - 2G_S\sigma_i + 2K\sigma_j\sigma_k - 2G_{IS}\tau_{3i}(\sigma_u - \sigma_d), \quad (2)$$

where $\sigma_i = \langle \bar{q}_i q_i \rangle$ stands for the quark condensate with (i, j, k) being any permutation of (u, d, s) , and τ_{3i} is the isospin quantum number of quark, i.e., $\tau_{3u} = 1$, $\tau_{3d} = -1$, and $\tau_{3s} = 0$. As shown in Eq. (2), σ_d and σ_s contribute to the u quark mass through the KMT interaction as well as the scalar-isovector coupling, called the flavor mixing [23, 24] in the constituent quark mass. The constituent quark mass M_i in vacuum is much larger than the current quark mass m_i , representing the spontaneous chiral symmetry breaking, while at high densities and/or temperatures M_i becomes approximately the same as m_i , representing the chiral symmetry restoration. In this way, the quark condensate or the constituent quark mass can serve as an order parameter for chiral phase transition. In the present study, the approximate chiral phase transition boundary is taken as where the light quark condensate is half of that in vacuum [8].

From the mean-field approximation and some algebras based on the finite-temperature field theory, the thermodynamic potential Ω_{NJL} of quark matter at finite temperature and quark chemical potential can be expressed as

$$\begin{aligned}
\Omega_{\text{NJL}} = & -2N_c \sum_{i=u,d,s} \int_0^\Lambda \frac{d^3p}{(2\pi)^3} [E_i + T \ln(1 + e^{-\beta(E_i - \tilde{\mu}_i)}) \\
& + T \ln(1 + e^{-\beta(E_i + \tilde{\mu}_i)})] + G_S(\sigma_u^2 + \sigma_d^2 + \sigma_s^2) \\
& - 4K\sigma_u\sigma_d\sigma_s + G_V(\rho_u^2 + \rho_d^2 + \rho_s^2) \\
& + G_{IS}(\sigma_u - \sigma_d)^2 + G_{IV}(\rho_u - \rho_d)^2. \quad (3)
\end{aligned}$$

In the above, the factor $2N_c$ represents the spin and color degeneracy, $\beta = 1/T$ represents the temperature, ρ_i is the net quark number density of flavor i ($i = u, d, s$), and $E_i(p) = \sqrt{p^2 + M_i^2}$ is the single quark energy. The effective chemical potential $\tilde{\mu}_i$ is defined as

$$\tilde{\mu}_i = \mu_i + 2G_V\rho_i + 2G_{IV}\tau_{3i}(\rho_u - \rho_d), \quad (4)$$

with the flavor mixing in $\tilde{\mu}_i$ similar to that in the constituent quark mass (Eq. (2)). The quark condensate can be expressed as

$$\sigma_i = -2N_c \int_0^\Lambda \frac{d^3p}{(2\pi)^3} \frac{M_i}{E_i} (1 - f_i - \bar{f}_i), \quad (5)$$

where

$$f_i = \frac{1}{1 + e^{\beta(E_i - \bar{\mu}_i)}}, \quad (6)$$

$$\bar{f}_i = \frac{1}{1 + e^{\beta(E_i + \bar{\mu}_i)}}, \quad (7)$$

are respectively the Fermi distribution functions of quarks and antiquarks. The net quark number density of the flavor i can be calculated from f_i and \bar{f}_i via

$$\rho_i = 2N_c \int_0^\Lambda (f_i - \bar{f}_i) \frac{d^3p}{(2\pi)^3}. \quad (8)$$

The above equations are solved self-consistently to obtain the quark matter properties at a given quark chemical potential and temperature.

The 3-flavor NJL model briefly reviewed above is effective in describing chiral phase transition but fails to get a deconfinement transition. The Polyakov loop, which was inspired by the strong-coupling analyses [25–28], has later been incorporated into the NJL model [29, 30] in order to compensate effectively the gluon contribution, and it can serve as an order parameter for deconfinement phase transition [29, 31].

The thermodynamic potential Ω_{pNJL} of the 3-flavor pNJL model at finite temperature and quark chemical potential can be expressed as

$$\begin{aligned} \Omega_{\text{pNJL}} = & \mathcal{U}(\Phi, \bar{\Phi}, T) - 2N_c \sum_i \int_0^\Lambda \frac{d^3p}{(2\pi)^3} E_i \\ & - 2T \sum_i \int \frac{d^3p}{(2\pi)^3} [\ln(1 + e^{-3\beta(E_i - \bar{\mu}_i)} \\ & + 3\Phi e^{-\beta(E_i - \bar{\mu}_i)} + 3\bar{\Phi} e^{-2\beta(E_i - \bar{\mu}_i)} \\ & + \ln(1 + e^{-3\beta(E_i + \bar{\mu}_i)} + 3\bar{\Phi} e^{-\beta(E_i + \bar{\mu}_i)} \\ & + 3\Phi e^{-2\beta(E_i + \bar{\mu}_i)})] + G_S(\sigma_u^2 + \sigma_d^2 + \sigma_s^2) \\ & - 4K\sigma_u\sigma_d\sigma_s + G_V(\rho_u^2 + \rho_d^2 + \rho_s^2) \\ & + G_{IS}(\sigma_u - \sigma_d)^2 + G_{IV}(\rho_u - \rho_d)^2, \quad (9) \end{aligned}$$

where the form of the temperature-dependent effective potential $\mathcal{U}(\Phi, \bar{\Phi}, T)$ as a function of the Polyakov loop Φ and $\bar{\Phi}$ is taken from Ref. [8] as

$$\begin{aligned} \mathcal{U}(\Phi, \bar{\Phi}, T) = & -b \cdot T \{ 54e^{-a/T} \Phi \bar{\Phi} + \ln[1 - 6\Phi \bar{\Phi} \\ & - 3(\Phi \bar{\Phi})^2 + 4(\Phi^3 + \bar{\Phi}^3)] \}. \quad (10) \end{aligned}$$

The parameters $a = 664$ MeV and $b = 0.015\Lambda^3$ are determined by the condition that the first-order phase transition in the pure gluodynamics takes place at $T = 270$ MeV, and the simultaneous crossover of chiral restoration and deconfinement phase transition occurs around $T \approx 200$ MeV [8]. The second integral in Eq. (9) is finite thus without the ultraviolet cutoff, different from the NJL model. In order to get the minimum of the thermodynamic potential Ω_{pNJL} , the following five equations are solved

$$\frac{\partial \Omega_{\text{pNJL}}}{\partial \sigma_u} = \frac{\partial \Omega_{\text{pNJL}}}{\partial \sigma_d} = \frac{\partial \Omega_{\text{pNJL}}}{\partial \sigma_s} = \frac{\partial \Omega_{\text{pNJL}}}{\partial \Phi} = \frac{\partial \Omega_{\text{pNJL}}}{\partial \bar{\Phi}} = 0,$$

leading to the values of σ_u , σ_d , σ_s , Φ , and $\bar{\Phi}$ in the pNJL model. The approximate deconfinement phase transition boundary is taken as where the Polyakov loop Φ is equal to 1/2 [8].

Starting from the thermodynamic potential, the energy density of the system can be obtained from the thermodynamical relation

$$\varepsilon = \Omega + \beta \frac{\partial}{\partial \beta} \Omega + \sum_i \mu_i \rho_i. \quad (11)$$

Accordingly, the energy density from the NJL model can be written as

$$\begin{aligned} \varepsilon_{\text{NJL}} = & -2N_c \sum_{i=u,d,s} \int_0^\Lambda \frac{d^3p}{(2\pi)^3} E_i (1 - f_i - \bar{f}_i) \\ & - \sum_{i=u,d,s} (\bar{\mu}_i - \mu_i) \rho_i + G_S(\sigma_u^2 + \sigma_d^2 + \sigma_s^2) \\ & - 4K\sigma_u\sigma_d\sigma_s + G_V(\rho_u^2 + \rho_d^2 + \rho_s^2) \\ & + G_{IS}(\sigma_u - \sigma_d)^2 + G_{IV}(\rho_u - \rho_d)^2 - \varepsilon_0. \quad (12) \end{aligned}$$

In the above expression, ε_0 is introduced to ensure $\varepsilon_{\text{NJL}} = 0$ in vacuum. Similarly, the energy density from the pNJL model can be expressed as

$$\begin{aligned} \varepsilon_{\text{pNJL}} = & 54abe^{-a/T} \Phi \bar{\Phi} + 2N_c \sum_{i=u,d,s} \int_\Lambda^\infty \frac{d^3p}{(2\pi)^3} E_i \\ & - 2N_c \sum_{i=u,d,s} \int \frac{d^3p}{(2\pi)^3} E_i (1 - F_i - \bar{F}_i) \\ & - \sum_{i=u,d,s} (\bar{\mu}_i - \mu_i) \rho_i + G_S(\sigma_u^2 + \sigma_d^2 + \sigma_s^2) \\ & - 4K\sigma_u\sigma_d\sigma_s + G_V(\rho_u^2 + \rho_d^2 + \rho_s^2) \\ & + G_{IS}(\sigma_u - \sigma_d)^2 + G_{IV}(\rho_u - \rho_d)^2 - \varepsilon_0, \quad (13) \end{aligned}$$

where

$$F_i = \frac{1 + 2\bar{\Phi}\xi_i + \Phi\xi_i^2}{1 + 3\bar{\Phi}\xi_i + 3\Phi\xi_i^2 + \xi_i^3} \quad (14)$$

and

$$\bar{F}_i = \frac{1 + 2\Phi\xi'_i + \bar{\Phi}\xi_i'^2}{1 + 3\Phi\xi'_i + 3\bar{\Phi}\xi_i'^2 + \xi_i'^3} \quad (15)$$

are the effective phase-space distribution functions for quarks and antiquarks in the pNJL model with $\xi_i = e^{(E_i - \bar{\mu}_i)/T}$ and $\xi'_i = e^{(E_i + \bar{\mu}_i)/T}$. One expects that the different effective phase-space distribution functions for quarks and antiquarks in the pNJL model may lead to different temperature effects on the thermodynamical quantities from the NJL model. The pressure for cold quark matter can be calculated from

$$P = \sum_{i=u,d,s} \mu_i \rho_i - \varepsilon_{\text{NJL}}, \quad (16)$$

which will be used in the study of compact stars.

III. ISOSPIN DEPENDENCE OF PHASE DIAGRAM

Most of our knowledge on the QCD phase diagram are restricted to zero isospin chemical potential $\mu_I = 0$. In relativistic heavy-ion collisions using neutron-rich nucleus beams, the hadron-quark phase transition is related to the phase diagram at nonzero μ_I or isospin asymmetry δ . In terms of different chemical potential μ_u for u quarks and μ_d for d quarks, the baryon chemical potential μ_B and the isospin chemical potential μ_I can be expressed respectively as

$$\frac{\mu_B}{3} = \frac{\mu_u + \mu_d}{2} = \mu, \quad \mu_I = \frac{\mu_u - \mu_d}{2}. \quad (17)$$

The isospin asymmetry δ in the quark phase can be defined as [32]

$$\delta = 3 \frac{\rho_d - \rho_u}{\rho_d + \rho_u}, \quad (18)$$

where the ρ_u and ρ_d are the net quark number densities for u and d quarks, respectively. The above definitions of the isospin chemical potential μ_I and the isospin asymmetry δ can be consistently related to those in nuclear matter

$$\mu_I = \frac{\mu_p - \mu_n}{2}, \quad (19)$$

$$\delta = \frac{\rho_n - \rho_p}{\rho_n + \rho_p}, \quad (20)$$

with μ_n and μ_p being the neutron and proton chemical potentials and ρ_n and ρ_p the corresponding number densities. By assuming that the ratio of electric/baryon charge, or equivalently the isospin asymmetry δ if the net strange quark number is zero, is conserved in relativistic heavy-ion collisions, the isospin asymmetry in the quark phase produced in central Au+Au collisions is thus

$$\delta = \frac{N - Z}{N + Z} = 0.198, \quad (21)$$

with $N = 118$ and $Z = 79$ being the neutron and proton numbers for Au nucleus, respectively. Due to the larger degeneracy of quarks than nucleons, the isospin chemical potential is much smaller in the quark phase than in the nucleon phase at the same isospin asymmetry, especially at lower temperatures. Similar to Refs. [23, 24, 33], we will study the QCD phase diagram at a fixed isospin chemical potential $\mu_I = -30$ MeV in addition to that at a fixed isospin asymmetry $\delta = 0.198$ in the following, while the net strange quark density ρ_s is assumed to be zero in both cases. We must note here that an isospin chemical potential as large as $\mu_I = -30$ MeV can not be reached so far in heavy-ion experiments according to our best knowledge, but it is always of theoretical interest to explore the QCD phase diagram at larger μ_I . We will also discuss the influence of the scalar-isovector and vector-isovector interactions on the isospin dependence of the

QCD phase diagram. For the ease of discussions, we define $R_{IS} = G_{IS}/G_S$ and $R_{IV} = G_{IV}/G_S$ as the reduced strength of the scalar-isovector and vector-isovector coupling. Since the NJL model can be considered as an effective field theory, R_{IS} and R_{IV} are treated as free parameters in the following studies.

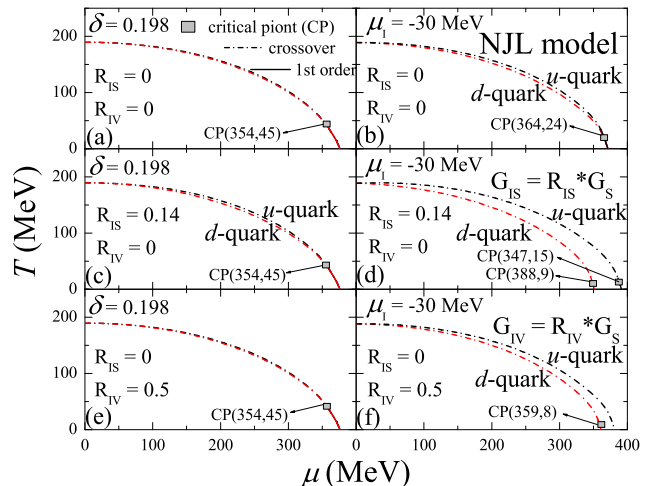


FIG. 1: (color online) Phase diagram in the $\mu - T$ plane of quark matter from the 3-flavor NJL model with various scalar-isovector and vector-isovector coupling constants at a fixed isospin asymmetry $\delta = 0.198$ (left) as in Au+Au collisions or at a fixed isospin chemical potential $\mu_I = -30$ MeV (right). The dash-dotted curves represent the approximate phase boundaries of a crossover transition while the solid lines are those of a first-order transition, with a critical point appearing in between.

We begin our discussion with the phase diagram from the 3-flavor NJL model. Figure 1 displays the phase diagram in the $\mu - T$ plane for various isovector coupling constants at a fixed isospin asymmetry or isospin chemical potential, and with zero net strange quark density. The left panels represent the phase diagram at the isospin asymmetry $\delta = 0.198$, and the critical point for the chiral phase transition is $(\mu = 354 \text{ MeV}, T = 45 \text{ MeV})$, representing the transition of the light quark condensate from a smooth change to a sudden jump at the phase boundary. It is seen that the QCD phase diagram is almost insensitive to the isovector couplings, as a result of the small isospin asymmetry or isospin chemical potential reached in Au+Au collisions. At a larger isospin chemical potential $\mu_I = -30$ MeV without isovector couplings (Panel (b)), the chiral phase transitions of u quark and d quark still share the similar boundary and the critical point, as a result of the flavor-mixing effect due to the six-point interaction which refers to the axial $U(1)_A$ symmetry anomaly [23]. With the increasing scalar-isovector coupling constant, the phase boundaries as well as the critical points of u and d quarks become to separate and their difference reaches the maximum around

$G_{IS} = 0.14G_S$, as shown in Panel (d), where the temperatures of the two critical points are also lower compared to the case without isovector couplings. The isospin splitting of the u and d quark chiral phase transition has also been observed in Refs. [23, 24, 33]. Further increase of R_{IS} leads to a negative d quark constituent mass near the phase boundary and will be discussed later. We find that for negative values of R_{IS} there is no separation of the u and d quark chiral phase transition and the critical point is similar to that without isovector couplings. We further display the effects of the vector-isovector coupling on the phase diagram in Panel (f), and observe similar effects as those from the scalar-isovector coupling, i.e., the isospin splitting of the chiral phase transition boundary is observed for positive R_{IV} , while for negative R_{IV} the phase diagram is the same as that without isovector couplings. For R_{IV} larger than 0.5, the d quark chemical potential near the phase boundary is comparable to the cutoff value Λ in the momentum integral, i.e., leading to the invalidity of the model. For positive R_{IS} or R_{IV} , it is also observed that the critical point for d quarks is always at a slightly smaller chemical potential compared with that for u quarks.

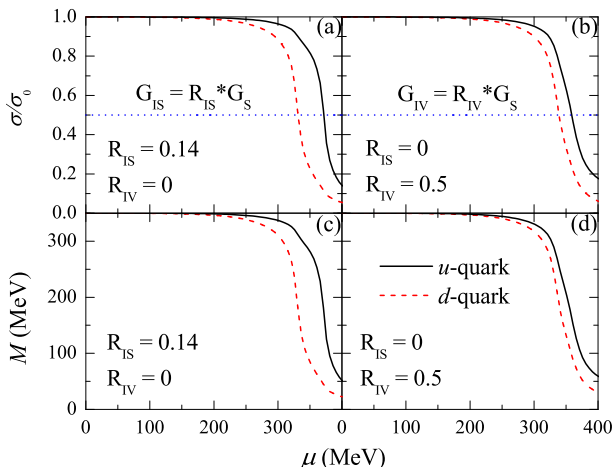


FIG. 2: (color online) The reduced quark condensates (upper panels) and the constituent masses (lower panels) of u and d quarks as a function of quark chemical potential at $T = 50$ MeV and $\mu_I = -30$ MeV with typical strength of scalar-isovector and vector-isovector couplings. σ_0 is the quark condensate in vacuum.

To understand the phase diagrams in Fig. 1, we show in Fig. 2 the reduced light quark condensate (upper panels) and the corresponding constituent quark mass (lower panels) at a typical temperature of $T = 50$ MeV and isospin chemical potential $\mu_I = -30$ MeV. The u quark condensate has a larger magnitude than the d quark condensate, resulting in a separate phase boundary at the chemical potential where the reduced quark condensate is $1/2$. The different u and d quark condensates lead to their different constituent quark masses according to Eq. (2), resulting in a larger u quark than d quark mass.

The isospin splitting of the constituent quark mass is important in isospin dynamics of relativistic heavy-ion collisions. For instance, if u and d quarks are affected by the same potential, d quarks will propagate faster. Positive values of R_{IS} lead to the enhancement of the isospin splitting of quark condensate as well as the constituent quark mass through the positive feedback mechanism, as can be seen from Eq. (2) that a larger difference between σ_u and σ_d leads to a larger difference between M_u and M_d , given that the quark condensate is negative. On the other hand, negative values of R_{IS} reduce the isospin splitting of quark condensate as well as that of the constituent quark mass through the negative feedback mechanism, leading to eventually the same phase boundary for u and d quarks. The values of R_{IS} greater than 0.14 lead to a too large isospin splitting and thus a negative d quark mass near the phase boundary. Similar mechanism applies to the vector-isovector coupling, but with reduced secondary effect.

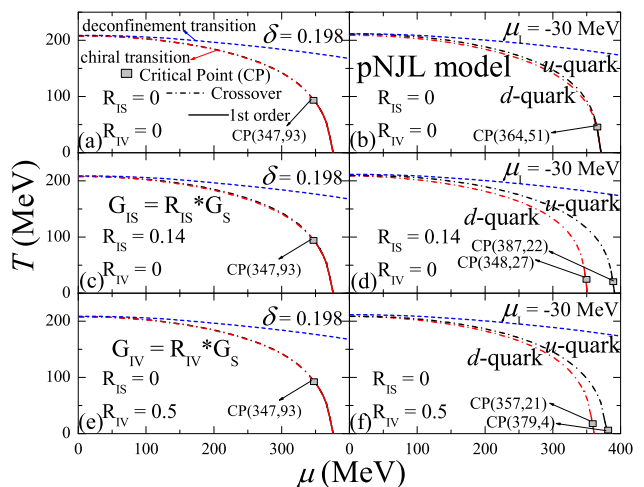


FIG. 3: (color online) Similar to Fig. 1 but from the 3-flavor pNJL model. The dashed lines represent the approximate phase boundary of a crossover deconfinement transition.

The effect of the Polyakov loop on the phase diagram in the μ - T plane is displayed in Fig. 3. As found in many other works [8, 9], the critical point moves to a higher temperature and a slightly smaller quark chemical potential ($\mu = 347$ MeV, $T = 93$ MeV) from the pNJL model at the isospin asymmetry $\delta = 0.198$ without isovector couplings, as exhibited in the left panels. The isospin effect on the QCD phase diagram with the Polyakov loop is still small in the quark system produced from Au+Au collisions. With isovector couplings at $\mu_I = -30$ MeV, the isospin splitting of the u and d quark chiral phase boundaries as well as their critical points is observed, qualitatively similar to the results from the NJL model. On the other hand, the temperatures of the critical points are also mostly increased in the pNJL model compared with those in Fig. 1. The approximate phase boundary of deconfinement transition is plotted, which is always a

crossover in the pNJL model and seems to be mostly independent of the isovector couplings. The region between the dashed line and the dash-dotted line was referred to as the quarkyonic phase in Refs. [8, 34–36], while a latest study found that the chiral symmetry can be broken in quarkyonic matter in an inhomogeneous way, which is called the quarkyonic chiral spirals [37, 38].

To summarize, the isospin effect on the QCD phase diagram is small with the small isospin asymmetry or isospin chemical potential reached in Au+Au collisions, while the isospin splitting of u and d quark chiral phase transition boundaries and critical points becomes considerable at a fixed larger isospin chemical potential $\mu_I = -30$ MeV. Since the quark condensate is the order parameter for chiral phase transition, the scalar-isovector coupling has the direct effect on the isospin splitting of u and d quark chiral phase transition boundaries and critical points, while the vector-isovector coupling has the similar but secondary effect. This can be understood from Eq. (2). The Polyakov loop doesn't affect the isospin dependence of the phase diagram but moves the critical point to higher temperatures.

IV. QUARK MATTER SYMMETRY ENERGY

The symmetry energy in nucleonic system, denoting the energy difference between isospin asymmetric and symmetric nuclear matter, has been a hot topic so far [11–17]. Since the quark matter in relativistic heavy-ion collisions at RHIC-BES or FAIR-CBM energies as well as in compact stars is isospin asymmetric, the quark matter symmetry energy is also an important quantity affecting the EOS of the system. It has been shown that the quark matter symmetry energy is important in understanding the properties of quark stars and explaining the observed two-solar-mass compact stars based on a confined-isospin-density-dependent-mass model [39]. On the other hand, the importance of the quark matter symmetry energy is not restricted to the fact that it is a piece of the EOS of the system, but it is related to the isospin splitting of u and d quark constituent mass as well as their different potentials, with the latter splitting as $\pm G_{IV}(\rho_u - \rho_d)$ in isospin asymmetric quark matter, through respectively the scalar-isovector and the vector-isovector coupling. This is similar to the case of nuclear matter symmetry energy which is related to the isospin splitting of neutron and proton in-medium effective mass as well as their mean-field potentials [14, 40].

Generally, the binding energy of quark matter consisting of u , d , and s quarks can be expanded in isospin asymmetry as

$$E(\rho_B, \delta, \rho_s) = E_0(\rho_B, \rho_s) + E_{sym}(\rho_B, \rho_s)\delta^2 + \vartheta(\delta^4). \quad (22)$$

In the above, $E_0(\rho_B, \rho_s) = E(\rho_B, \delta = 0, \rho_s)$ is the binding energy per baryon number in the 3-flavor quark matter with equal number of u and d quarks and net s quark number density ρ_s , and $\rho_B = (\rho_u + \rho_d + \rho_s)/3$ is the

net baryon number density. The quark matter symmetry energy $E_{sym}(\rho_B, \rho_s)$, standing as the second-order coefficient in the expansion of the isospin asymmetry, is expressed by definition as

$$E_{sym}(\rho_B, \rho_s) = \frac{1}{2!} \frac{\partial^2 E(\rho_B, \delta, \rho_s)}{\partial \delta^2} \Big|_{\delta=0}. \quad (23)$$

Note that the definition of the quark matter symmetry energy in the present study has been generalized to finite-temperature systems containing both quarks and anti-quarks. Neglecting the contribution from higher-order terms in Eq. (22) for small δ , the quark matter symmetry energy can also be calculated approximately from

$$E_{sym}(\rho_B, \rho_s) \approx \frac{E(\rho_B, \delta, \rho_s) - E(\rho_B, \delta = 0, \rho_s)}{\delta^2}, \quad (24)$$

where $\delta = 0.05$ is used in the calculation. One sees that $E_{sym}(\rho_B, \rho_s)$ depends on both ρ_B and ρ_s , corresponding to the interplay between the isospin and the strangeness sectors.

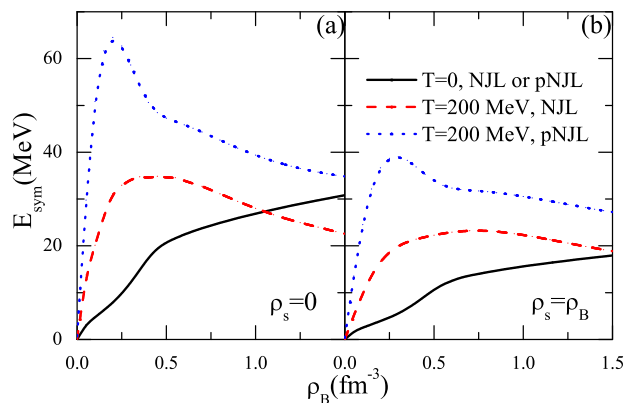


FIG. 4: (color online) Quark matter symmetry energy from the 3-flavor NJL and pNJL model with strange quark density $\rho_s = 0$ (left) and $\rho_s = \rho_B$ (right) at $T = 0$ and $T = 200$ MeV without isovector couplings.

We begin the discussion with the quark matter symmetry energy E_{sym} by comparing that from the NJL model and the pNJL model without isovector couplings, as displayed in Fig. 4, with results from $\rho_s = 0$ in the left panel and $\rho_s = \rho_B$ in the right panel. At zero temperature when the pNJL model reduces to the NJL model, E_{sym} increases monotonically with increasing ρ_B , while at $T = 200$ MeV it first increases then slightly decreases with increasing ρ_B . The density and temperature dependence of E_{sym} are not so simple, but we found that there are always dramatic changes of the quantities near the chiral transition phase boundary. The quark matter symmetry energy is much enhanced in the pNJL model at $T = 200$ MeV, especially at lower densities, compared to that in the NJL model. The larger quark matter symmetry energy in the pNJL model than in the NJL model is

mainly due to their different kinetic energy contributions, as a result of larger isospin splitting of u and d quark constituent masses as well as a more diffusive phase-space distribution function in the pNJL model. On the other hand, E_{sym} is reduced in the presence of strange quarks for both NJL model and pNJL model, and the density is rescaled, i.e., the whole curve moves to the high-density side since in this case we have $\rho_B = \frac{1}{2}(\rho_u + \rho_d)$ instead of $\rho_B = \frac{1}{3}(\rho_u + \rho_d)$.

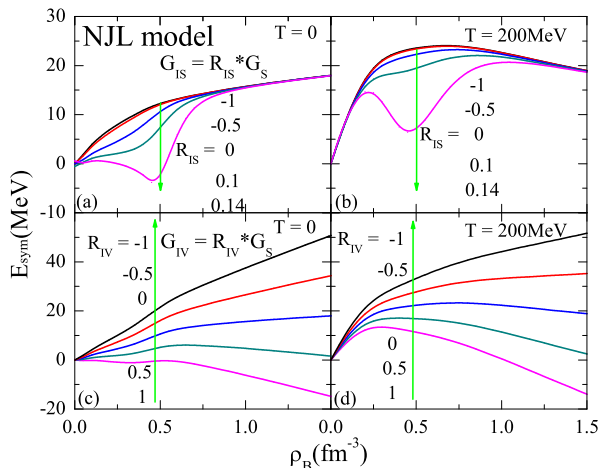


FIG. 5: (color online) Quark matter symmetry energy for different scalar-isovector (upper panels) and vector-isovector (lower panels) coupling constants at $T = 0$ (left panels) and 200 MeV (right panels) from the 3-flavor NJL model with $\rho_s = \rho_B$.

The quark matter symmetry energy for various isovector coupling constants from the 3-flavor NJL model with $\rho_s = \rho_B$ is displayed in Fig. 5. Qualitatively, E_{sym} decreases with increasing constant of both the scalar-isovector and vector-isovector couplings. It is seen that E_{sym} is sensitive to the scalar-isovector coupling only at intermediate densities when the difference between the u and d quark condensate is large, and it exhibits a strong decrease for $R_{IS} = 0.14$ when that difference is largest. In addition, E_{sym} decreases linearly with increasing R_{IV} . The sensitivity of E_{sym} on the scalar-isovector and vector-isovector couplings can be understood respectively from Eq. (12) that the first flavor summation overwhelms the $G_{IS}(\sigma_u - \sigma_d)^2$ term and the second flavor summation overwhelms the $G_{IV}(\rho_u - \rho_d)^2$ term, based on some algebras. The temperature effect on E_{sym} is larger at lower ρ_B while smaller at higher ρ_B .

Figure 6 displays the quark matter symmetry energy from the 3-flavor pNJL model with $\rho_s = \rho_B$. Again, the dependence of the scalar-isovector and vector-isovector coupling on E_{sym} is qualitatively similar to that from the NJL model. On the other hand, except for the case with a positive R_{IS} , E_{sym} is mostly enhanced in the pNJL model compared with that in the NJL model, especially

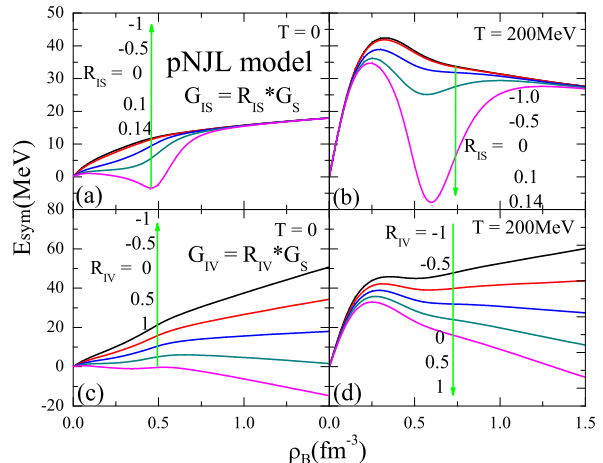


FIG. 6: (color online) Same as Fig. 5 but from the 3-flavor pNJL model.

at lower baryon densities.

To summarize, the vector-isovector coupling has the direct effect on the quark matter symmetry energy, while the scalar-isovector coupling has the secondary effect. This can be understood from Eq. (12). The Polyakov loop mostly enhances the quark matter symmetry energy, compared with that from the NJL model, and this is mainly due to the different kinetic contributions.

We would also like to emphasize here that we take the scalar-isovector coupling G_{IS} and the vector-isovector coupling G_{IV} as the two sources of the quark matter symmetry energy, in addition to the naive kinetic contribution. On the other hand, G_{IS} and G_{IV} can lead to other isospin effects in addition to the quark matter symmetry energy, such as the u and d quark constituent mass splitting. Once we know the quark matter symmetry energy and some other microscopic properties of quark matter, we can have a global picture of quark interactions. This could be achieved by comparing results from transport model simulations using the NJL Lagrangian with available experimental data in the near future.

V. APPLICATIONS TO HYBRID STARS

The quark matter symmetry energy obtained above can be important in understanding properties of compact stars with quark degree of freedom. It has been shown [20] that the vector-isovector coupling has considerable effects on the EOS of strange quark star matter, a β -equilibrium and charge-neutral system containing u , d , and s quarks as well as leptons. Here we apply the present model to hybrid stars, with a quark core at high densities, a mixed phase of quarks and hadrons at moderate densities, and a hadronic phase at low densities. The possible appearance of hyperons is neglected and in this

work we mainly focus on the quark matter effects on the properties of hybrid stars.

In the high-density quark phase, the system consists of a mixture of quarks (u , d , and s) and leptons (e and μ) at charge neutrality and β -equilibrium condition, i.e.,

$$\frac{2}{3}\rho_u - \frac{1}{3}(\rho_d + \rho_s) - \rho_e - \rho_\mu = 0 \quad (25)$$

and

$$\mu_i = \mu_B b_i - \mu_c q_i, \quad (26)$$

with μ_B and μ_c being the baryon and charge chemical potential, and q_i and b_i being the charge and baryon number of particle species i , respectively. For quarks, the energy density (ε_Q) and the pressure (P_Q) can be obtained based on the NJL model from Eqs. (12) and (16), respectively. For leptons, we take both electrons and muons as free Fermi gas with their masses $m_e = 0$ and $m_\mu = 106$ MeV, respectively, and their energy density and pressure can be expressed as

$$\varepsilon_L = \sum_{i=e,\mu} \frac{1}{\pi^2} \int_0^{k_F^i} \sqrt{k^2 + m_i^2} k^2 dk, \quad (27)$$

$$P_L = \sum_{i=e,\mu} \mu_i \rho_i - \varepsilon_L. \quad (28)$$

The total energy density and pressure of the high-density quark phase in hybrid stars including the contributions from both quarks and leptons are given by

$$\varepsilon^Q = \varepsilon_Q + \varepsilon_L, \quad (29)$$

$$P^Q = P_Q + P_L. \quad (30)$$

In the low-density hadronic phase, an isospin- and momentum-dependent effective nuclear interaction is used to describe the β -equilibrium and charge-neutral neutron star matter, with the single-particle potential written as [41, 42]

$$\begin{aligned} U_\tau(\rho, \delta, \vec{p}) &= A_u \frac{\rho_{-\tau}}{\rho_0} + A_l \frac{\rho_\tau}{\rho_0} \\ &+ B \left(\frac{\rho}{\rho_0} \right)^\sigma (1 - x\delta^2) - 4\tau x \frac{B}{\sigma + 1} \frac{\rho^{\sigma-1}}{\rho_0^\sigma} \delta \rho_{-\tau} \\ &+ \frac{2C_l}{\rho_0} \int d^3 p' \frac{f_\tau(\vec{r}, \vec{p}')}{1 + (\vec{p} - \vec{p}')^2 / \Lambda^2} \\ &+ \frac{2C_u}{\rho_0} \int d^3 p' \frac{f_{-\tau}(\vec{r}, \vec{p}')}{1 + (\vec{p} - \vec{p}')^2 / \Lambda^2}. \end{aligned} \quad (31)$$

In the above, $\tau = 1(-1)$ for neutrons (protons) is the isospin index, ρ_n and ρ_p are number densities of neutrons and protons, respectively, the isospin asymmetry δ is defined as $\delta = (\rho_n - \rho_p)/\rho$, with $\rho = \rho_n + \rho_p$ being the total number density, and $f_\tau(\vec{r}, \vec{p})$ is the nucleon phase-space distribution function. The seven parameters (A_l , A_u , B , C_l , C_u , Λ , σ) are fitted by empirical constraints of nuclear

matter properties at the saturation density, and their detailed values can be found in Ref. [42]. In the present study we set $x = 0$ corresponding to a moderately stiff nuclear matter symmetry energy. The chemical potential of neutrons and protons can be calculated from

$$\mu_\tau = \sqrt{m^2 + p_\tau^{F^2}} + U_\tau(\rho, \delta, p_\tau^F), \quad (32)$$

with m the nucleon mass and $p_\tau^F = (3\pi^2 \rho_\tau)^{1/3}$ the Fermi momentum. The total energy density and pressure of the low-density hadronic phase in hybrid stars including the contributions from both nucleons and leptons are given by

$$\varepsilon^H = \varepsilon_H + \varepsilon_L, \quad (33)$$

$$P^H = P_H + P_L, \quad (34)$$

where the detailed expressions for the energy density ε_H and pressure P_H of nuclear matter can be found in Ref. [46].

At moderate densities of hybrid stars, the Gibbs construction method [43, 44] is applied to construct the hadron-quark mixed phase, with the β -equilibrium, the baryon number conservation, and the charge neutrality conditions respectively expressed as

$$\mu_i = \mu_B b_i - \mu_c q_i, \quad (35)$$

$$\rho_B = (1 - Y)(\rho_n + \rho_p) + \frac{Y}{3}(\rho_u + \rho_d + \rho_s), \quad (36)$$

$$0 = (1 - Y)\rho_p + \frac{Y}{3}(2\rho_u - \rho_d - \rho_s) - \rho_e - \rho_\mu, \quad (37)$$

where Y is the baryon number fraction of the quark phase. The total energy density and pressure of the mixed phase are calculated according to

$$\varepsilon^M = (1 - Y)\varepsilon_H + Y\varepsilon_Q + \varepsilon_L, \quad (38)$$

$$P^M = (1 - Y)P_H + YP_Q + P_L. \quad (39)$$

The core-crust transition density as well as the crust EOS in hybrid stars are also treated properly according to Refs. [45, 46]. The whole EOS from low to high densities is used to study the mass-radius relation of hybrid stars through the Tolman-Oppenheimer-Volkoff (TOV) equations [47]. Technical details of the study can be found in Ref. [48] except that the quark matter is now described by the 3-flavor NJL model.

As described above, compact stars are different systems compared with heavy-ion collisions. The latter has a short lift time, a higher temperature, and zero net strangeness, while the former is a stable cold system with particle species determined from the β -equilibrium and charge neutrality condition. Investigating the two systems could be helpful in understanding the quark interaction from different points of view.

Before discussing the EOS, we first display the particle fractions in hybrid stars in the whole density range in Fig. 7. With various isovector coupling strength, the

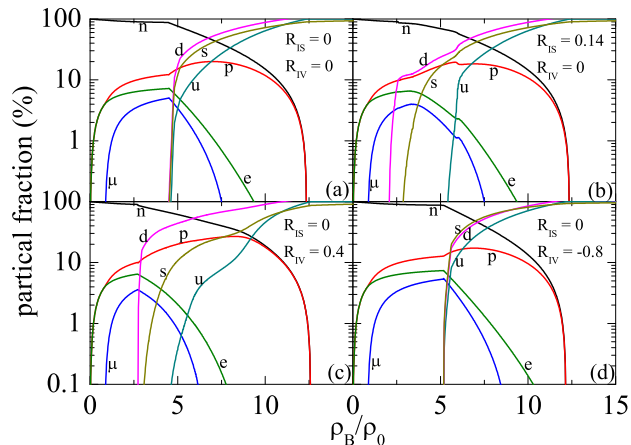


FIG. 7: (color online) Particle fractions of neutrons (n), protons (p), electrons (e), muons (μ), u quarks (u), d quarks (d), and s quarks (s) in hybrid star matter with quark matter properties described by the 3-flavor NJL model from various isovector coupling constants.

hadron-quark mixed phase appears around $3 \sim 5 \rho_0$ and disappears at $\rho_B > 10\rho_0$, where leptons are largely suppressed. For positive isovector coupling constants, quarks of different flavors appear at different densities and their fractions are quite different, especially for the positive vector-isovector coupling constants which directly affects the quark chemical potential via Eq. (4). For negative isovector coupling constants, quarks of different flavors appear at almost the same density, similar to the case without isovector coupling, as a result of negative isospin feedback mechanism discussed in Sec. III. It is also observed that quarks generally appear at higher densities for negative isovector coupling constants compared with positive ones.

The density dependence of the isospin chemical potential μ_I and the isospin asymmetry δ in hybrid stars is illustrated in Fig. 8, where μ_I turns out to be half of the charge chemical potential μ_c , and the isospin asymmetry in the mixed phase is calculated from [32]

$$\delta = \frac{(1 - Y)(\rho_n - \rho_p) + Y(\rho_d - \rho_u)}{\rho_B}, \quad (40)$$

with ρ_B defined by Eq. (36). It is seen that the isospin chemical potential drops to as low as -115 MeV in the hadronic phase, while it begins to increase when quarks appear. Although the isospin chemical potential is small in pure quark phase, it can still be large in the mixed phase. For the isospin asymmetry, it is close to 1 at lower densities, but keeps on decreasing with increasing baryon density. One sees from Fig. 8 that the quark system with large isospin chemical potentials or isospin asymmetries can exist in the mixed phase of hybrid stars. This is the existing system with the largest isospin chemical potential we know so far, but with zero temperature and finite

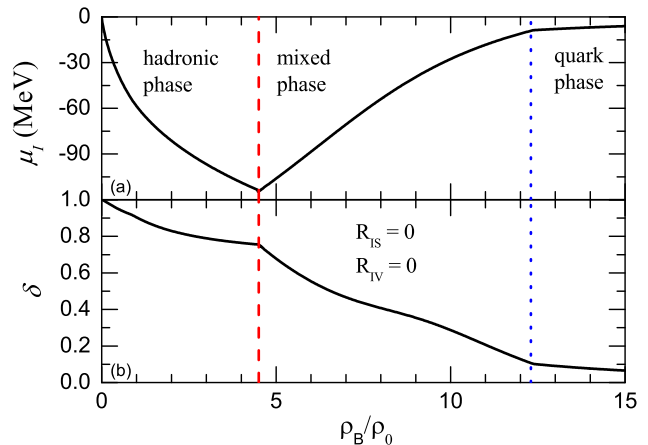


FIG. 8: (color online) Density dependence of the isospin chemical potential μ_I (a) and the isospin asymmetry δ (b) in hybrid stars with quark phase described by the 3-flavor NJL model without isovector couplings.

net strange quark densities, different from the situation mentioned in Sec. III.

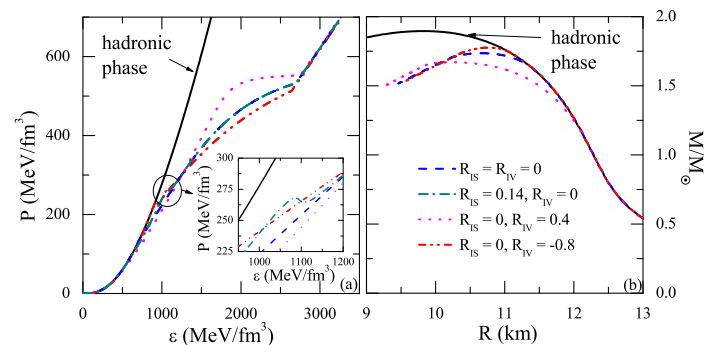


FIG. 9: (color online) The EOS (left) and the mass-radius relation (right) of hybrid stars for various isovector coupling constants in the quark phase described by the 3-flavor NJL model.

Figure 9 displays the EOS and the mass-radius relation for the corresponding hybrid stars from various isovector coupling constants used in Fig. 7, and the result from pure hadronic phase is also shown for comparison. Interestingly, we observe a spinodal behavior in the EOS from $R_{IS} = 0.14$ in the hadron-quark mixed phase, as shown in the inset, exhibiting that the corresponding hybrid star is unstable. This can be understood from Fig. 5 where a positive scalar-isovector coupling leads to a significant decrease of the quark matter symmetry energy at intermediate densities. Although not shown here, we observe that the result from a negative R_{IS} is almost the same as that without isovector coupling. A negative R_{IV} leads to the later appearance of quarks and thus a stiffer EOS at intermediate densities as shown in the inset, although

at higher densities a positive R_{IV} somehow leads to a larger pressure. As a result, a negative vector-isovector coupling gives the largest maximum mass of hybrid stars (approximately 1.8 solar mass), which is still smaller than that of the observed massive compact stars.

VI. POSSIBLE EFFECTS FROM BREAKING THE STRANGENESS SECTOR

Since introducing the isovector coupling in the 3-flavor NJL model more breaks the strangeness SU(3) symmetry than the isospin SU(2) symmetry, here we briefly discuss the possible effects on the isospin properties of quark matter discussed in the previous sections if we further introduce the scalar-strangeness and vector-strangeness couplings in the NJL Lagrangian

$$\begin{aligned} \mathcal{L}_{\text{NJL}} \rightarrow \mathcal{L}_{\text{NJL}} &+ G_{SS}[(\bar{q}\lambda_8 q)^2 + (\bar{q}i\gamma_5\lambda_8 q)^2] \\ &+ G_{SV}[(\bar{q}\gamma_\mu\lambda_8 q)^2 + (\bar{q}\gamma_5\gamma_\mu\lambda_8 q)^2] \end{aligned} \quad (41)$$

where G_{SS} and G_{SV} are the corresponding coupling constants. As a consequence, the constituent mass, effective chemical potential, thermodynamic potential, and energy density for the 3-flavor NJL model are modified to

$$M_i \rightarrow M_i - 2s_i G_{SS}(\sigma_u + \sigma_d - 2\sigma_s), \quad (42)$$

$$\tilde{\mu}_i \rightarrow \tilde{\mu}_i + 2s_i G_{SV}(\rho_u + \rho_d - 2\rho_s), \quad (43)$$

$$\begin{aligned} \Omega_{\text{NJL}} \rightarrow \Omega_{\text{NJL}} &+ G_{SS}(\sigma_u + \sigma_d - 2\sigma_s)^2 \\ &+ G_{SV}(\rho_u + \rho_d - 2\rho_s)^2, \end{aligned} \quad (44)$$

$$\begin{aligned} \varepsilon_{\text{NJL}} \rightarrow \varepsilon_{\text{NJL}} &+ G_{SS}(\sigma_u + \sigma_d - 2\sigma_s)^2 \\ &+ G_{SV}(\rho_u + \rho_d - 2\rho_s)^2, \end{aligned} \quad (45)$$

with $s_i = 1$ for u and d quarks and $s_i = -2$ for s quarks.

Employing a fixed isospin chemical potential $\mu_I = -30$ MeV and $G_{IS} = G_{IV} = 0$, we display in Fig. 10 the phase diagram for various strangeness coupling constants with $\rho_s = 0$ and $\rho_s = \rho_B$ from the 3-flavor NJL model. Again we introduce $R_{SS} = G_{SS}/G_S$ and $R_{SV} = G_{SV}/G_S$ as the reduced scalar-strangeness and vector-strangeness coupling strength, and they are treated as free parameters. As σ_s is much larger than σ_u or σ_d near the chiral phase boundary, the constituent quark mass is mostly negative for a positive R_{SS} , which is not shown here. On the other hand, for a negative R_{SS} the chiral phase transition at $\mu = 0$ happens at a higher temperature, compared to the case without strangeness coupling. With finite net strange quark density $\rho_s = \rho_B$, it is seen that generally the chiral phase boundary moves to the small- μ side, and the isospin splitting of the chiral phase boundaries for u and d quarks is also slightly reduced, compared to the case with $\rho_s = 0$, as a result of the interplay between the isospin and strangeness sectors. Again, the isospin splittings are more considerable from the scalar-strangeness coupling than from the vector-strangeness coupling, consistent with our findings in the previous sections. Generally, the critical point barely exists for a negative strangeness coupling constant, while a positive

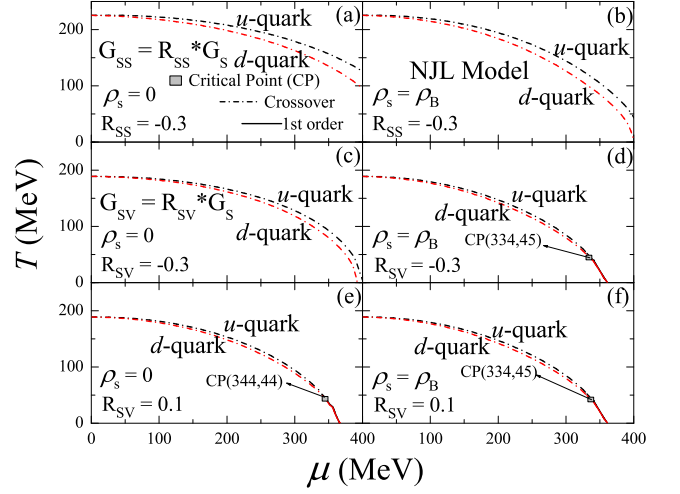


FIG. 10: (color online) Phase diagram in the $\mu - T$ plane for various scalar-strangeness and vector-strangeness coupling constants with $\rho_s = 0$ (left) and $\rho_s = \rho_B$ (right) at a fixed isospin chemical potential $\mu_I = -30$ MeV from the 3-flavor NJL model. The dash-dotted curves represent the approximate phase boundaries of a crossover transition while the solid lines are those of a first-order transition, with a critical point appearing in between.

vector-strangeness coupling constant favors the existence of the critical point.

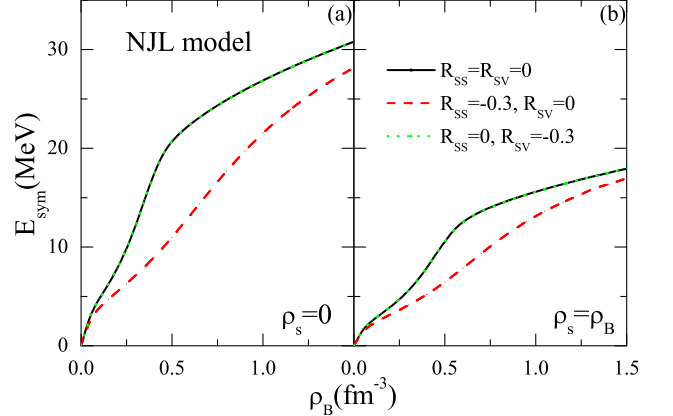


FIG. 11: (color online) Quark matter symmetry energy from the 3-flavor NJL model with strange quark density $\rho_s = 0$ (left) and $\rho_s = \rho_B$ (right) at zero temperature with various coupling constants of the strangeness sector.

We have also studied the effects of the strangeness coupling on the quark matter symmetry energy, which are displayed in Fig. 11. The vector-strangeness coupling has no effect on the quark matter symmetry energy, since the $(\rho_u + \rho_d - 2\rho_s)^2$ term is independent of the isospin asymmetry δ . Although the scalar-strangeness coupling has no direct contribution to the potential part of the symmetry energy, it modifies the isospin splitting of u and d quark constituent mass and reduces the quark matter symmetry

energy by affecting the kinetic part. Again, the symmetry energy is reduced in the presence of strange quarks as found in Sec. IV. The EOS of isospin asymmetric quark matter is related to the quark matter symmetry energy, and it is found that the vector-strangeness coupling has little effect on the hybrid star results discussed above while the scalar-strangeness coupling slightly reduces the maximum mass of hybrid stars.

VII. CONCLUSIONS AND OUTLOOK

In this work, we have studied the properties of isospin asymmetric quark matter based on the 3-flavor Nambu-Jona-Lasinio model as well as its Polyakov-loop extension with scalar-isovector and vector-isovector couplings. Although the isospin effect on the phase diagram has been found small with the isospin asymmetry reached in high-energy heavy-ion collisions, considerable isospin effect is observed at a fixed isospin chemical potential $\mu_I = -30$ MeV, which can not be reached in heavy-ion experiments so far. The separation of the u and d quark chiral phase transition is observed with positive isovector coupling constants but is suppressed with negative ones. The quark matter symmetry energy is shown to decrease with increasing isovector coupling constant, and is mostly enhanced with Polyakov-loop extension. We found that the isospin splittings of quark condensate, constituent quark mass, and chiral phase transition as well as the critical point are more sensitive to the scalar-isovector coupling, while the quark matter symmetry energy is more sensitive to the vector-isovector coupling. A positive scalar-isovector coupling constant can lead to an unstable isospin asymmetric quark matter and hybrid star matter. The particle fraction as well as the equation of state in hybrid stars depends on the isovector couplings as well. Possible effects on the above results from further breaking of the strangeness sector among the flavor symmetry have also been discussed.

At RHIC-BES or FAIR-CBM energies, the isospin splitting of final hadron observables is expected to be sensitive to the isospin dynamics of the produced quark

matter. In the spirit of Ref. [49], by comparing the experimental results of such splitting with those from transport model simulations based on the NJL Lagrangian used in the present work, one can in principle extract useful information of the isospin dependence of the QCD phase diagram and constrain the quark matter symmetry energy. In addition, the method of calculating the QCD phase diagram used in the present study is valid only for small isospin chemical potentials ($|\mu_I| < m_\pi/2$). To explore the whole 3-dimensional QCD phase diagram at larger isospin chemical potentials, one needs to introduce an additional order parameter of pion condensate [50–54]. Such studies will be carried out in the future.

Acknowledgments

We thank Che Ming Ko and Feng Li for helpful discussions, and the anonymous referee for providing useful comments and suggestions with great patience. JX acknowledges support from the Major State Basic Research Development Program (973 Program) of China under Contract No. 2015CB856904 and No. 2014CB845401, the National Natural Science Foundation of China under Grant No. 11475243 and No. 11421505, the "100-Talent Plan" of Shanghai Institute of Applied Physics under Grant No. Y290061011 and No. Y526011011 from the Chinese Academy of Sciences, the Shanghai Key Laboratory of Particle Physics and Cosmology under Grant No. 15DZ2272100, and the "Shanghai Pujiang Program" under Grant No. 13PJ1410600. LWC acknowledges the Major State Basic Research Development Program (973 Program) in China under Contract No. 2013CB834405 and No. 2015CB856904, the National Natural Science Foundation of China under Grant No. 11275125 and No. 11135011, the "Shu Guang" project supported by Shanghai Municipal Education Commission and Shanghai Education Development Foundation, the Program for Professor of Special Appointment (Eastern Scholar) at Shanghai Institutions of Higher Learning, and the Science and Technology Commission of Shanghai Municipality (11DZ2260700).

-
- [1] C. Bernard, T. Burch, C. Detar *et al.*, Phys. Rev. D **71**, 034504 (2005).
 - [2] Y. Aoki, G. Endrodi, Z. Fodor *et al.*, Nature **443**, 675 (2006).
 - [3] A. Bazavov, T. Bhattacharya, T. Cheng *et al.*, Phys. Rev. D **85**, 054503 (2012).
 - [4] I. Barbour, N. E. Behlil, E. Dagotto *et al.*, Nucl. Phys. B **275**, 296 (1986).
 - [5] F. Karsch, Lect. Notes Phys. **583**, 209 (2002).
 - [6] S. Muroya, A. Nakamura, C. Nonaka, and T. Takaishi, Prog. Theor. Phys. **110**, 615 (2003).
 - [7] M. Asakawa and K. Yazaki, Nucl. Phys. A **504**, 668 (1989).
 - [8] K. Fukushima, Phys. Rev. D **77**, 114028 (2008) [Erratum-ibid. D **78**, 039902 (2008)].
 - [9] S. Carignano, D. Nickel, and M. Buballa, Phys. Rev. D **82**, 054009 (2010).
 - [10] N. M. Bratovic, T. Hatsuda, and W. Weise, Phys. Lett. B **719**, 131 (2013).
 - [11] V. Baran *et al.*, Phys. Rep. **410**, 335 (2005).
 - [12] A. W. Steiner *et al.*, Phys. Rep. **411**, 325 (2005).
 - [13] J. M. Lattimer and M. Prakash, Phys. Rep. **442**, 109 (2007).
 - [14] B. A. Li, L. W. Chen, and C. M. Ko, Phys. Rep. **464**, 113 (2008).
 - [15] M. B. Tsang *et al.*, Prog. Part. Nucl. Phys. **66**, 400

- (2011).
- [16] J. M. Lattimer, *Annu. Rev. Nucl. Part. Sci.* **62**, 485 (2012).
- [17] C. J. Horowitz *et al.*, *J. Phys. G* **41**, 093001 (2014).
- [18] P. B. Demorest, T. Pennucci, S. M. Ranson, M. S. E. Roberts, and J. W. T. Hessels, *Nature* **467**, 1081 (2010).
- [19] J. Antoniadis, P. C. C. Freire, N. Wex, T. M. Tauris, R. S. Lynch, M. H. van Kerkwijk, M. Kramer, and C. Bassa *et al.*, *Science* **340**, 6131 (2013).
- [20] P. C. Chu, X. Wang, L. W. Chen, and M. Huang, *Phys. Rev. D* **91**, 023005 (2015); P. C. Chu, PhD thesis.
- [21] M. F. M. Lutz, S. Klimt, and W. Weise, *Nucl. Phys. A* **542**, 521 (1992).
- [22] M. Buballa, *Phys. Rep.* **407**, 205 (2005).
- [23] M. Frank, M. Buballa, and M. Oertel, *Phys. Lett. B* **562**, 221 (2003).
- [24] Z. Zhang and H. P. Su, *Phys. Rev. D* **80**, 054020 (2014).
- [25] A. Gocksch and M. Ogilvie, *Phys. Rev. D* **31**, 877 (1985).
- [26] E. M. Ilgenfritz and J. Kripfganz, *Z. Phys. C* **29**, 79 (1985).
- [27] A. Mocsy, F. Sannino, and K. Tuominen, *Phys. Rev. Lett.* **92**, 182302 (2004).
- [28] S. Digal, E. Laermann, and H. Satz, *Eur. Phys. J. C* **18**, 583 (2001).
- [29] K. Fukushima, *Phys. Lett. B* **591**, 277 (2004).
- [30] C. Ratti, M. A. Thaler, and W. Weise, *Phys. Rev. D* **73**, 014019 (2006).
- [31] K. Fukushima and T. Hatsuda, *Rep. Prog. Phys.* **74**, 014001 (2011).
- [32] M. Di Toro, B. Liu, V. Greco, V. Baran, M. Colonna, and S. Plumari, *Phys. Rev. C* **83**, 014911 (2011).
- [33] D. Toublan and J.B. Kugot, *Phys. Lett. B* **564**, 211 (2003).
- [34] C. Sasaki, B. Friman, and K. Redlich, *Phys. Rev. D* **75**, 074013 (2007).
- [35] L. McLerran and R.D. Pisarski, *Nucl. Phys. A* **796**, 83 (2007).
- [36] L. Ya. Glozman and R. F. Wagenbrunn, *Phys. Rev. D* **77**, 054027 (2008).
- [37] T. Kojo, Y. Hidaka, L. McLerran, and R. D. Pisarski, *Nucl. Phys. A* **843**, 37 (2010).
- [38] T. Kojo, R. D. Pisarski, and A. M. Tsvelik, *Phys. Rev. D* **82**, 074015 (2010).
- [39] P. C. Chu and L. W. Chen, *Astrophys. J.* **780**, 135 (2014).
- [40] B. A. Li and X. Han, *Phys. Lett. B* **727**, 276 (2013).
- [41] C. B. Das, S. Das Gupta, C. Gale, and B. A. Li, *Phys. Rev. C* **67**, 034611 (2003).
- [42] L. W. Chen, C. M. Ko, and B. A. Li, *Phys. Rev. Lett.* **94**, 032701 (2005).
- [43] N. K. Glendenning, *Phys. Rev. D* **46**, 1274 (1992).
- [44] N. K. Glendenning, *Phys. Rep.* **342**, 393 (2001).
- [45] J. Xu, L. W. Chen, B. A. Li, and H. R. Ma, *Phys. Rev. C* **79**, 035802 (2009).
- [46] J. Xu, L. W. Chen, B. A. Li, and H. R. Ma, *Astrophys. J.* **697**, 1549 (2009).
- [47] J. Oppenheimer and G. Volkoff, *Phys. Rev.* **55**, 374 (1939).
- [48] J. Xu, L.W. Chen, C. M. Ko, and B. A. Li, *Phys. Rev. C* **81**, 055803 (2010).
- [49] J. Xu, T. Song, C. M. Ko, and F. Li, *Phys. Rev. Lett.* **112**, 012301 (2014).
- [50] D. T. Son and M. A. Stephanov, *Phys. Rev. Lett.* **86**, 592 (2001).
- [51] B. Klein, D. Toublan, and J. J. M. Verbaarschot, *Phys. Rev. D* **68**, 014009 (2003).
- [52] A. Barducci, R. Casalbuoni, G. Pettini, and L. Ravagli, *Phys. Rev. D* **69**, 096004 (2004).
- [53] T. Sasaki, Y. Sakai, H. Kouno, and M. Yahiro, *Phys. Rev. D* **82**, 116004 (2010).
- [54] T. Xia, L. Y. He, and P. F. Zhuang, *Phys. Rev. D* **88**, 056013 (2013).